GROUND MOTION PREDICTION FOR THRUST EARTHQUAKES

P. SOMERVILLE[1] AND N. ABRAHAMSON[2]
[1]Woodward-Clyde Federal Services, Pasadena, Ca
[2] Consultant, Castro Valley, CA

ABSTRACT

In previous studies, the ground motion for reverse faults has been distinguished from the ground motion from strike-slip faults by a style-of-faulting factor in the attenuation relation. In most studies, this style-of-faulting factor has been assumed to be constant for all magnitudes, distances, and periods; however, some studies have examined these factors but not all together. The empirical ground motions for thrust faults are evaluated by developing a model for the magnitude, distance, and period dependence of the style-of-faulting factor. In developing the distance dependence, we distinguish between sites on the hanging wall from those on the foot wall, and from sites off the edge of the fault rupture. We find that there is a strong magnitude dependence of the style-of-faulting factor with smaller magnitude events producing a larger style-of-faulting factor. A strong distance dependence is found: sites over the hanging wall at distances of 8 to 18 km have an additional increase in ground motion of up to 50%; sites on the foot wall at distances of 12-30 km have a reduction of the ground motion of about 35%. No systematic period dependence is found over the period range of 0.03 to 5 seconds for sites off the ends of the rupture (not over the hanging wall or foot wall), but a strong period dependence is found for sites over the hanging wall and foot wall with smaller style-of-faulting factors at long periods (T> 1 sec).

INTRODUCTION

Recent empirical attenuation relation studies have generally found that peak horizontal accelerations from thrust earthquakes are 20-30% larger than from strike-slip earthquakes for the same magnitude and closest distance (e.g. Campbell 1993; Idriss 1991; Sadigh et al, 1993; Boore et al, 1994). This effect of earthquake mechanism on the ground motion has been called the style-of-faulting factor. For most attenuation relations, the style-of-faulting factor is simply a scale factor that is applied at all magnitudes and distances, and often the style-of-faulting factor derived for peak acceleration is assumed to apply to response spectral values at all periods as well.

Boore et al. (1994) estimated the style-of-faulting factor independently for each period for period of 0.1 to 2.0 seconds (plus PGA). They found that the style-of-faulting factor was not strongly dependent on period but did show a reduction at long periods (Figure 1A). Campbell and Bozorgnia (1994) examined the distance and magnitude dependence of the style-of-faulting factor for peak acceleration. They found that the style-of-faulting factor decreased with increasing magnitude and distance (Figure 1B), but they did not distinguish between sites on the hanging wall from those on the footwall.

Thrust earthquakes typically occur on non-vertically dipping faults. For dipping faults, the ground motion is not expected to be the same on both sides of the fault. Based on simple geometry alone, we expect that sites located above the fault rupture on the hanging wall will have larger ground motions than sites at the same rupture distance located on the foot wall because the hanging wall sites are closer to a larger area of the source than the foot wall sites (Figure 2) . This difference in the proximity of the source to the site is a result in part of using the shortest distance to the rupture plane as the definition of the closest distance. (Note that the distance measure used by Boore et al. accommodates some of the hanging wall and foot wall effects due to its definition.

For fault ruptures that do not reach the surface, we define the separation between the hanging wall and foot wall by the vertical projection of the top of the rupture plane (Figure 2). Using this definition, the hanging wall and foot wall motions must become equal for sites located directly over the top edge of the fault. Therefore, it does not make sense to simple estimate separate hanging wall and foot wall style-of-faulting factors. To do so would create a discontinuity at the surface projection of the top of the rupture. Sites off the edge of the fault rupture are excluded from the hanging wall and foot wall effects for this study (Figure 2).

As part of the CSMIP study, we are examining the magnitude and distance dependence of the style-of-faulting factor using both empirical data analyses and numerical simulations. In this paper, the preliminary results of the empirical data analysis are presented.

APPROACH

The magnitude and distance dependence of the style-of-faulting factor is evaluated by examining the residuals of the ground motion from attenuation relations. The full data set is used to develop the attenuation relations and then the residuals are examined to quantify the systematic differences in the ground motions for reverse and strike-slip events and for hanging wall and foot wall sites.

The data set used in this analysis is from the study of Abrahamson and Silva (1995) and consists of 685 recordings from 56 earthquakes including events up to the 1994 Northridge earthquake. To avoid potentially significant structure effects on the recorded ground motions, recordings from buildings that are greater than two stories in height were excluded from the data set. For all of the ground motion parameters used in this study, the geometric average of the ground motion on the two horizontal components is used.

The regression analysis is performed using the random effects algorithm as described by Abrahamson and Youngs (1992). The random effects model explicitly accounts for the correlations between recordings from the same earthquake. Conceptually, the random effects model finds an optimal weighting scheme (between equal weight to each record and equal weight to each earthquake) based on the given sampling of the data. The random effects model can be interpreted as estimating an event term (random effect) for each earthquake and in this sense it is similar to the two-step procedure used by Boore et al (1994).

PEAK ACCELERATION

An initial reference ground motion attenuation relation (without a distinction between reverse and strike-slip earthquakes) is developed. The residuals of the horizontal peak acceleration from this reference model are shown in Figure 3. These residuals are the mean event residuals including the eta term and the mean residual-eta for each event. This figure shows a magnitude dependence to the style-of-faulting factor similar to that found by Campbell and Bozorgnia (1994). We also found that the reverse oblique events yielded high frequency ground motions between the strike-slip and reverse events, but closer to the reverse events. On average, the style-of-faulting factor for reverse oblique events is about 70% of that of reverse events (at frequencies above 2 Hz). For this study, we will also use a magnitude dependent style-of-faulting factor as given below:

$$f_F(M) = \begin{cases} a_1 & M<5 \\ a_1 - (a_1-a_2)(M-5)/1.5 & 5.0 < M < 6.5 \\ a_2 & M \geq 6.5 \end{cases}$$

After adding the magnitude dependent style-of-faulting factor to the regression equation, the residuals were computed to examine the distance dependence (Figure 4). To distinguish between sites on the hanging wall and sites on the foot wall, the footwall sites are plotted at negative distances and the hanging wall sites are plotted at positive distances. As can be seen in this figure, the peak acceleration residuals on the hanging wall are biased to positive values for the distance range of 10 to 30 km (e.g. the attenuation model under predicts these peak accelerations); the residuals on the foot wall are biased to negative values over the distance range of 10-50 km.

Based on the trends in the residuals (Figure 4), the following piece wise continuous functional form is used for the distance dependence of the style-of-faulting factor on the hanging wall:

$$f_{HW}(r) = \begin{cases} 0 & \text{for } 0 \le r \le x_1 \\ b_1 \dfrac{(r-x_1)}{x_2-x_1} & \text{for } x_1 < r < x_2 \\ b_1 & \text{for } x_2 \le r \le x_3 \\ b_1\left(1 - \dfrac{(r-x_3)}{x_4-x_3}\right) & \text{for } x_3 < r < x_4 \\ 0 & \text{for} \end{cases}$$

where $f_{HW}(r)$ is the hanging wall effect. The boundary distances, x_1, x_2, x_3, and x_4 were estimated by visual inspection of the trends of the residuals. With the boundary distances fixed, the constant coefficient, b_1, was then estimated by regression. A similar model is used for the footwall sites with coefficients b_2, x_5, x_6, x_7, and x_8. The resulting parameter values are listed in Tables 2 and 3.

The resulting model is plotted in Figure 5. The results of the regression show that for sites located at closest distances of 8 to 18 km on the hanging wall the peak acceleration is about 50% larger than at sites off the ends of the fault at the same closest distance.

SPECTRAL CONTENT

The spectral values were also studied to estimate the period dependence on the style-of-faulting factor. The regression analysis was performed on the normalized spectra values (Sa/pga) because this approach helps to constrain the results to give a smooth spectral shape. In this study, we want to model effects that have a smooth and systematic period dependence. An initial regression is performed at each spectral period independently and then the period dependence of the resulting coefficients is examined to determine if the coefficient does vary smoothly and systematically with period.

The period dependence of the coefficients for the magnitude dependence of the style-of-faulting factor is shown in Figure 6. This figure shows that the magnitude dependence does not have a systematic trend with period. Therefore, we adopt a period independent magnitude dependence of the style-of-faulting factor (shown in Figure 5A).

The second effect to examine is the period dependence of the hanging wall and foot wall effects. The period dependence of the coefficients for the distance dependence of the style-of-

faulting factor is shown in Figure 7. This figure indicates that there is a systematic reduction in the Hanging wall / Foot wall effect at long periods. This indicates that the spectral content of reverse earthquakes is different from that of strike-slip earthquakes for sites located over the hanging wall or foot wall.

DISCUSSION

The impact of the distance dependence of the style-of-faulting factor on peak acceleration and 1 Hz spectral acceleration attenuation relations is shown in Figure 8. This figure shows the average rock site attenuation for M=7.0 strike-slip events, reverse events (at sites not over the fault), and reverse events for sites on the hanging wall and foot wall. The flat attenuation from 4 to 8 km on the hanging wall is expected to be a recurring feature of ground motions from reverse events which should be considered in seismic hazard analyses in regions with thrust faults. We expect that a similar effect would be observed for normal faulting events, but there is not enough strong motion data from normal faulting events to test this. The reduction in the footwall motions is not as well determined as the increase on the hanging wall. The 1 Hz attenuation shows a similar hanging wall effect as peak acceleration (but somewhat less) and a larger reduction on the foot wall. The reduction on the footwall should be used with caution until the final results of this study are available, including the numerical simulation results.

ACKNOWLEDGMENTS

This work was supported by grants from the Data Interpretation Project of the CDMG Strong Motion Instrumentation Program.

REFERENCES

Abrahamson, N. A. and W. Silva (1995). A consistent set of attenuation relations, Poster at SSA meeting in El Paso.

Abrahamson, N. A. and R. R. Youngs (1992). A stable algorithm for regression analyses using the random effects model, Bull. Seism. Soc. Am., 82, 505-510.

Boore, Joyner, and Fumal (1994). Ground motion estimates for strike- and reverse-slip faults, personal communication.

Campbell, K. W. (1993). Empirical prediction of near-source ground motion from large earthquakes, Proc. International Workshop on Earthquake Hazard and Large Dams in the Himalaya, January 15-16, 1993, New Delhi, India.

Campbell, K. W. and Y. Bozorgnia (1994). Near-source attenuation of peak horizontal acceleration from workwide accelerograms recorded from 1957 to 1993, Proc. Fifth National Conf. Earthquake Eng., III, 283-192.

Idriss, I. M. (1991). Selection of earthquake ground motions at rock sites, Report prepared for the Structures Div., Building and Fire Research Lab., NIST.

Sadigh, K., C-Y Chang, N. A. Abrahamson, S. J. Chiou, and M. S Power (1993). Specification of long period ground motions: updated attenuation relationships for rock site conditions and adjustment factors for near-fault effects, Proc. ATC 17-1, Seminar on Seismic Isolation, Passive Energy Dissipation, and Active Control, Vol I, 59-70.

Table 1. Events Used Analysis of Hanging Wall / Foot Wall Effects (M>6.0)

				Number of Recordings	
Event	**M**	**Dip**	**Mech**	**Foot**	**Hang**
1952 Kern County	7.4	67	RV	1	0
1971 San Fernando	6.6	53	RV	3	1
1976 Gazli	6.8	38	RV	0	1
1978 Tabas	7.4	30	RV	1	2
1983 Coalinga	6.5	32	RV	0	2
1985 Nahanni	6.8	23	RV	1	2
1989 Loma Prieta	7.0	70	OBL	6	3
1992 Cape Mendocino	7.1	13	RV	0	3
1994 Northridge	6.7	42	RV	7	10

Table 2. Coefficients for Hanging Wall Effects

Parameter	**Value**
x_1	4
x_2	8
x_3	18
x_4	25
x_5	-6
x_6	-12
x_7	-25
x_8	-50

Table 3. Coefficients for Style-of-Faulting Factor

period	**a_1**	**a_2**	**b_1**	**b_2**
0.0	0.58	0.27	0.38	-0.29
0.1	0.58	0.27	0.38	-0.29
0.2	0.58	0.27	0.38	-0.29
0.3	0.58	0.27	0.38	-0.35
0.4	0.58	0.27	0.38	-0.41
0.5	0.58	0.27	0.38	-0.48
0.75	0.58	0.27	0.35	-0.59
1.0	0.58	0.27	0.28	-0.64
2.0	0.58	0.27	0.10	-0.64
3.0	0.58	0.27	0.00	-0.64
4.0	0.58	0.27	0.00	-0.64

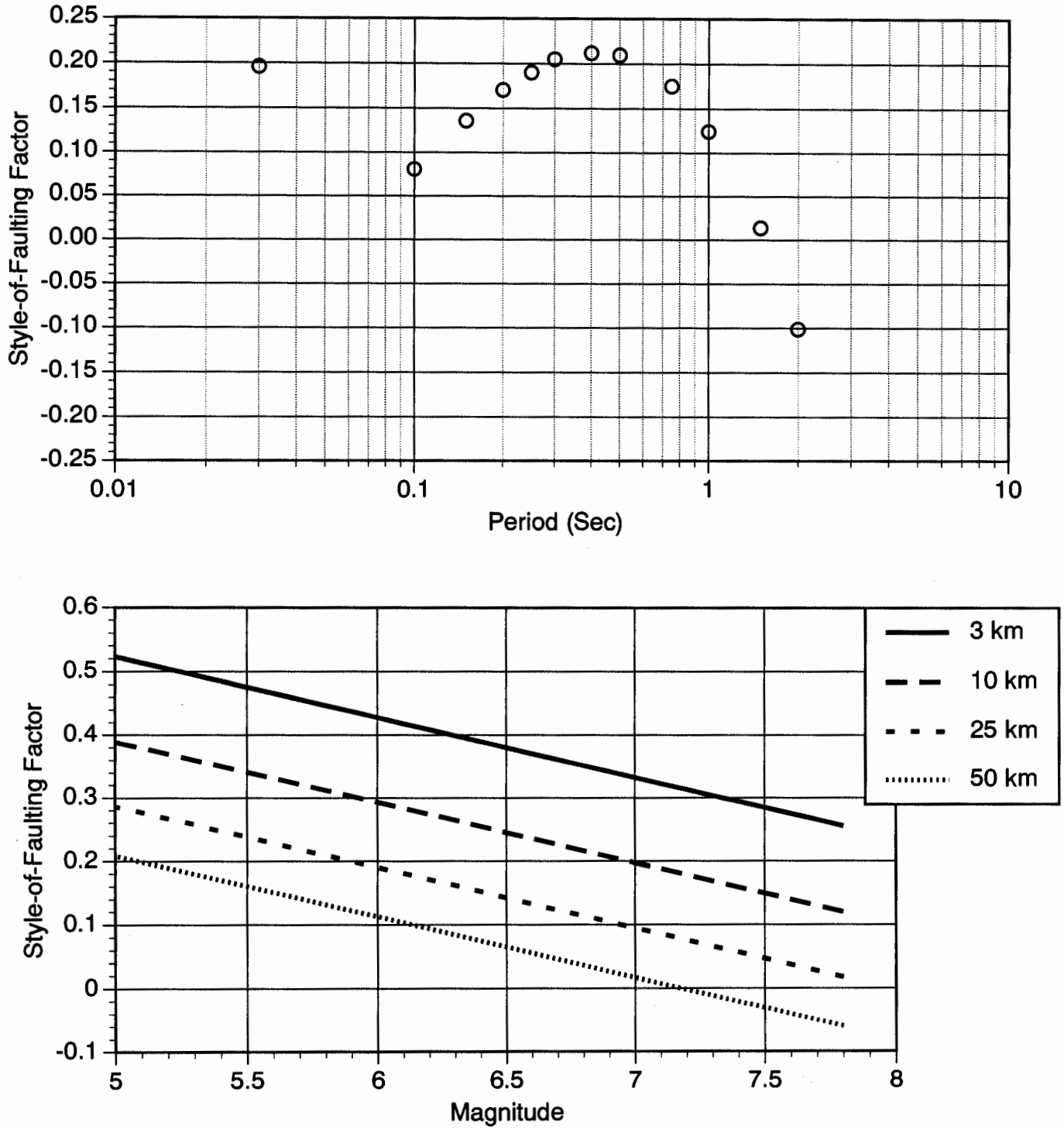

Figure 1. (A) Period dependence of the style-of-faulting factor estimated by Boore et al. (1994). (B) Magnitude and distance dependence of the style-of-faulting factor estimated by Campbell and Bozorgnia (1994).

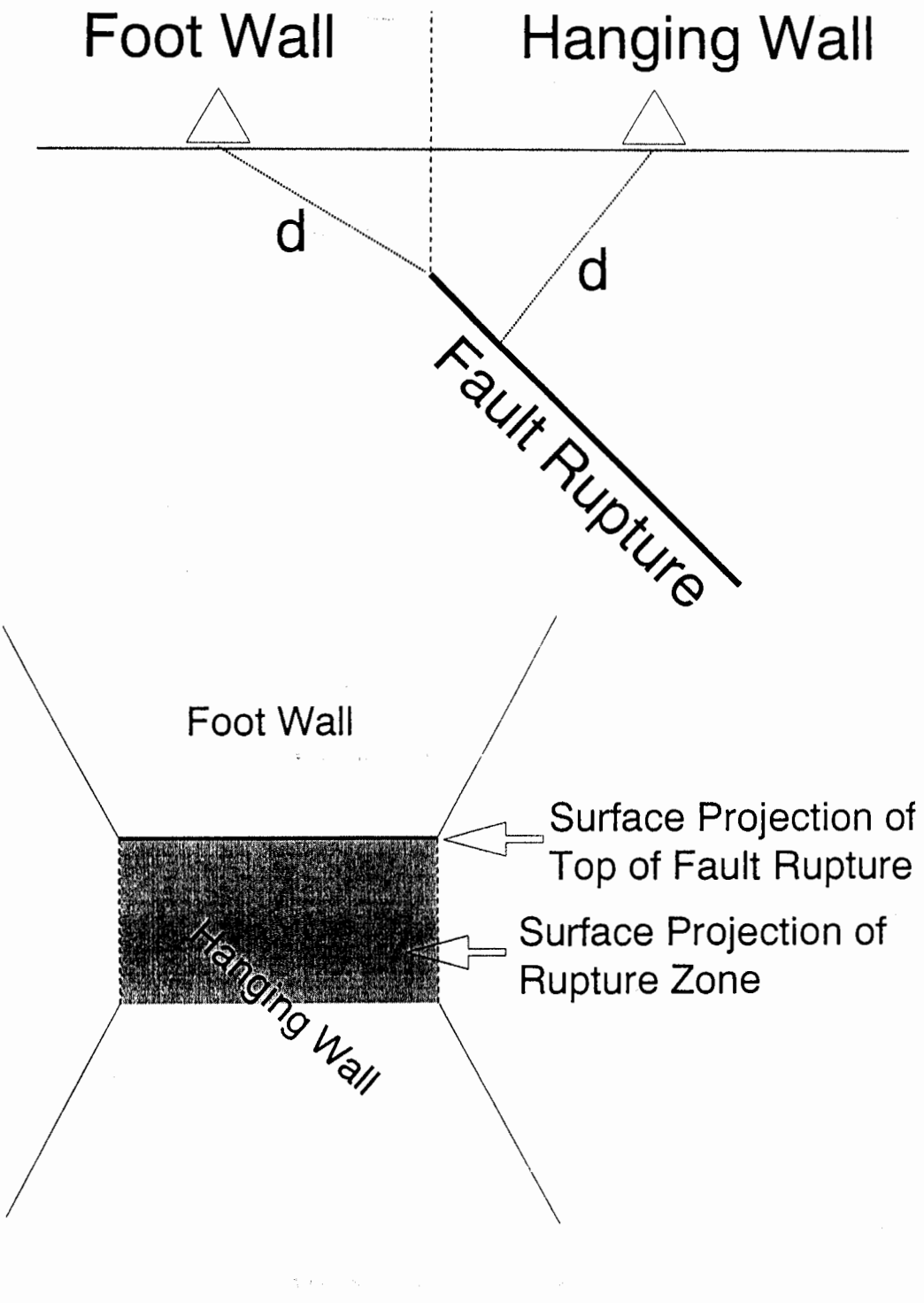

Figure 2. Classification of the stations into hanging wall and foot wall sites is based on the geometry shown above. The dividing line is the vertical projection of the top of the rupture (top frame). Sites off the ends of the fault are not included as either foot wall or hanging wall sites (lower frame).

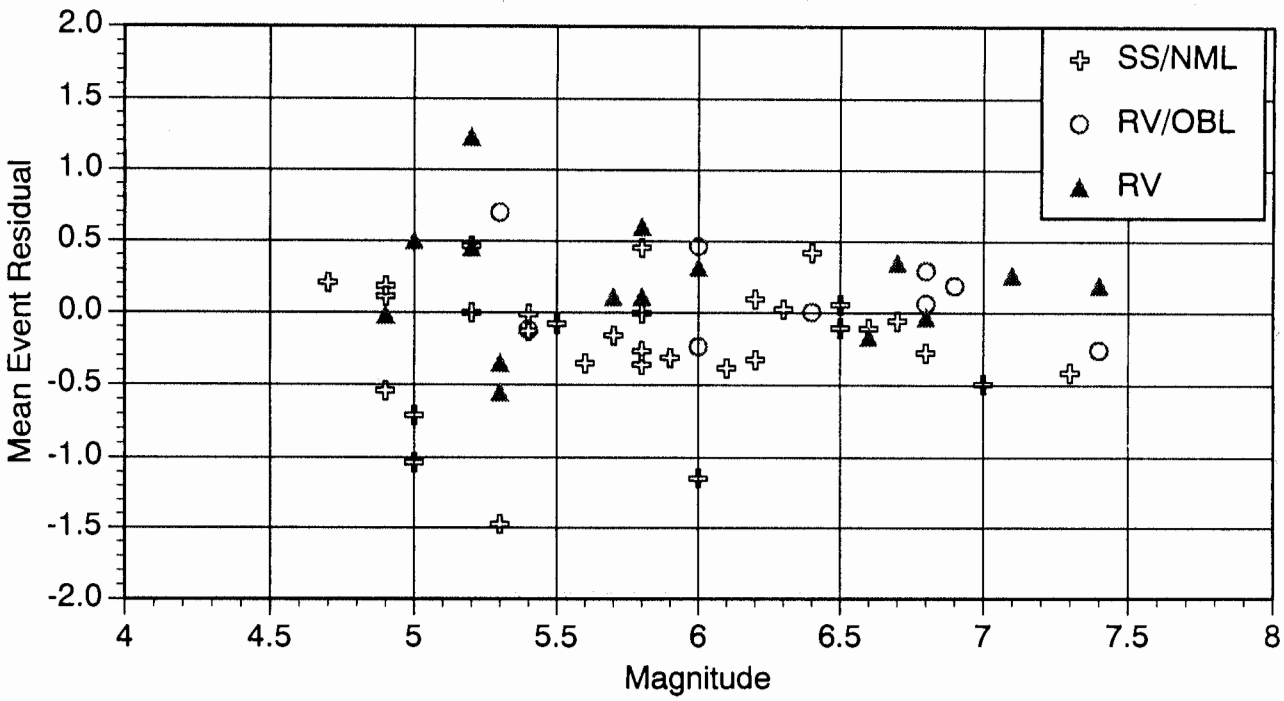

Figure 3. Mean event terms for peak acceleration (without a style-of-faulting factor in the regression).

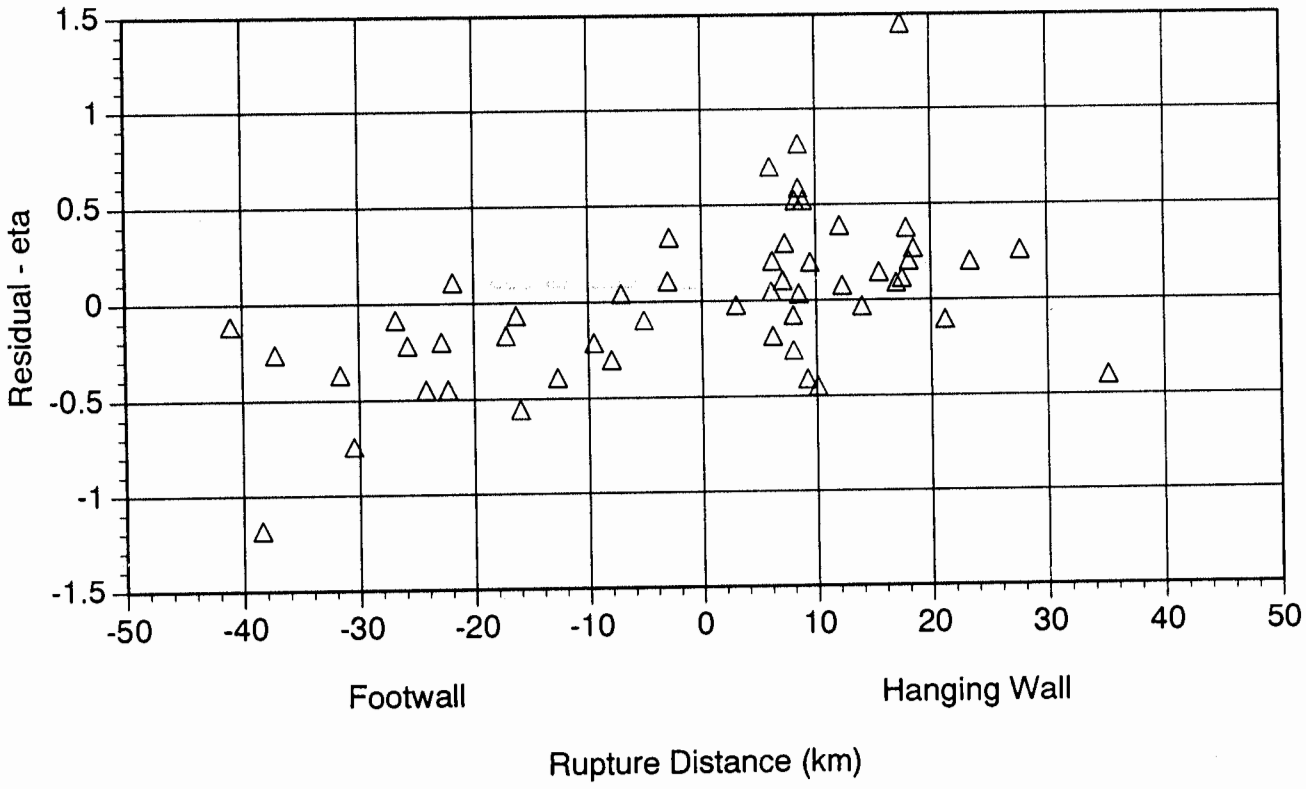

Figure 4. Peak acceleration residuals from a regression with a magnitude dependent style-of-faulting factor but without a distance dependent term.

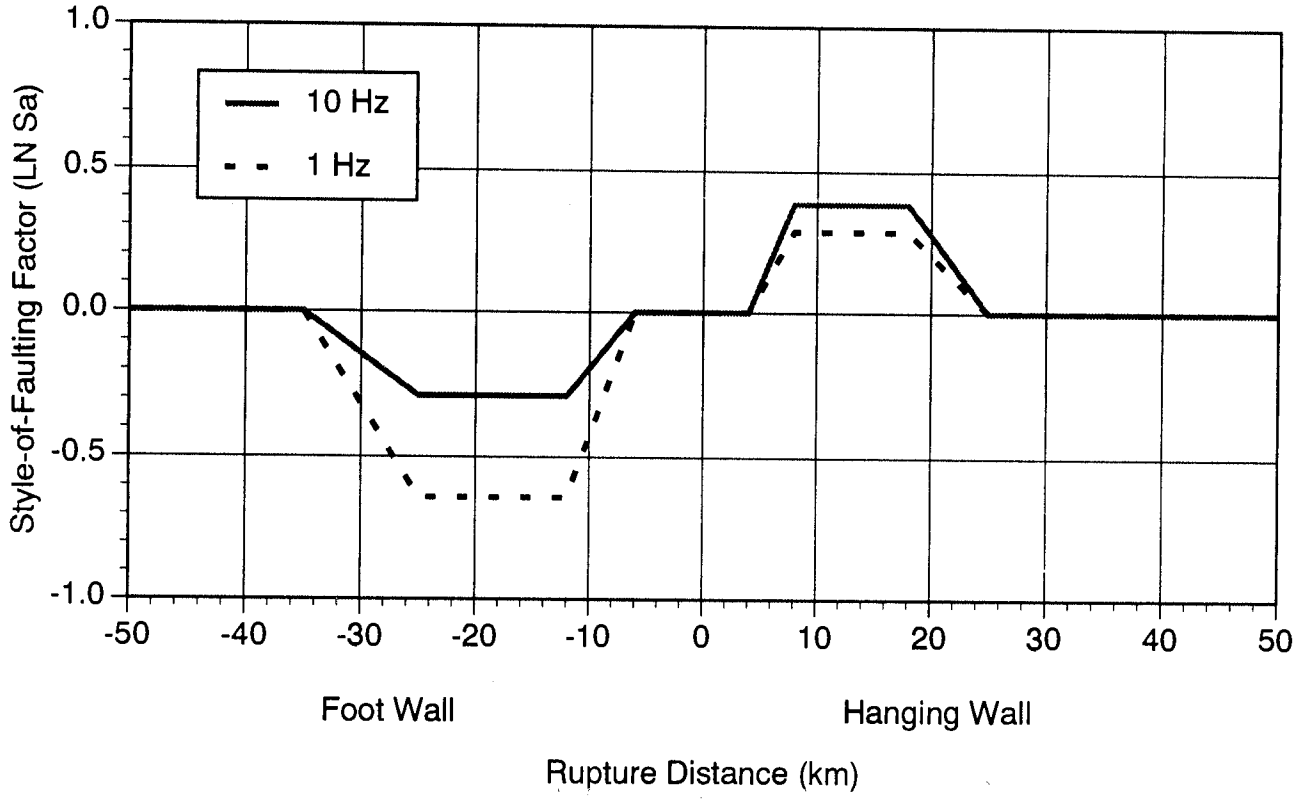

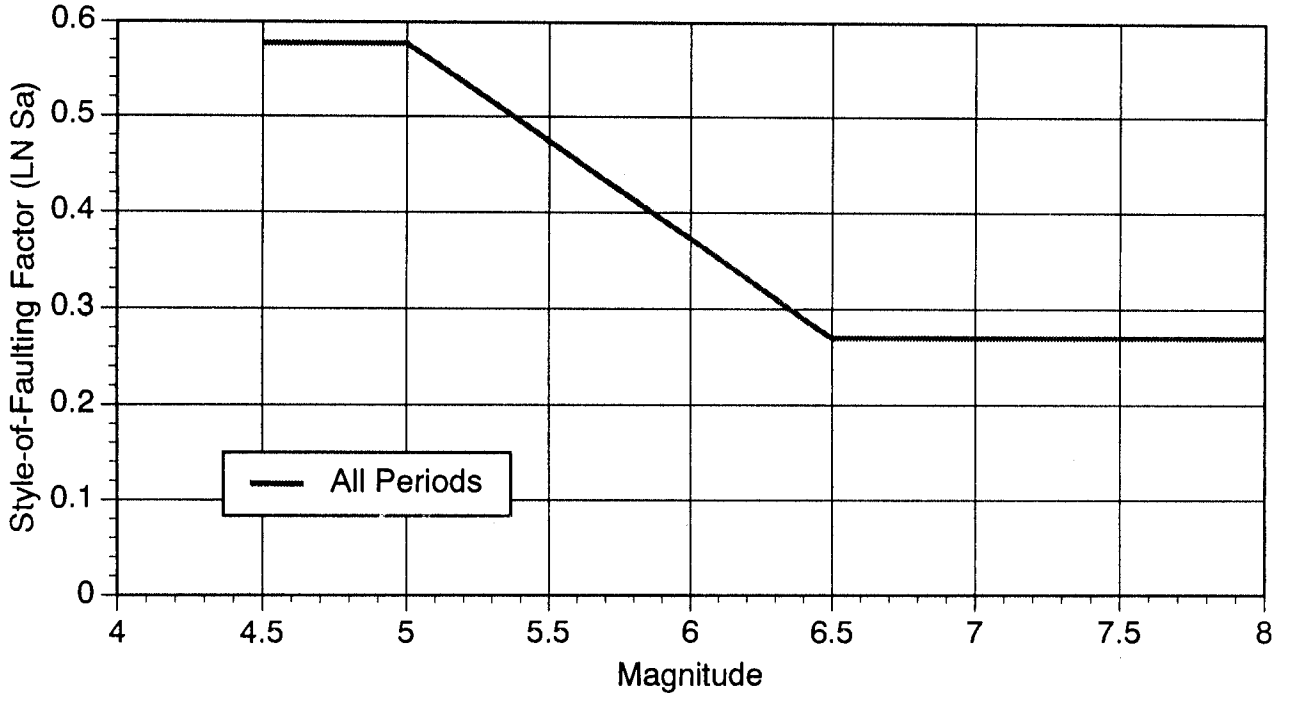

Figure 5. Magnitude dependence of the style-of-faulting factor (lower frame) and effect of the hanging wall and foot wall (top frame). The 10 Hz value for the HW/FW effect also applies to peak acceleration.

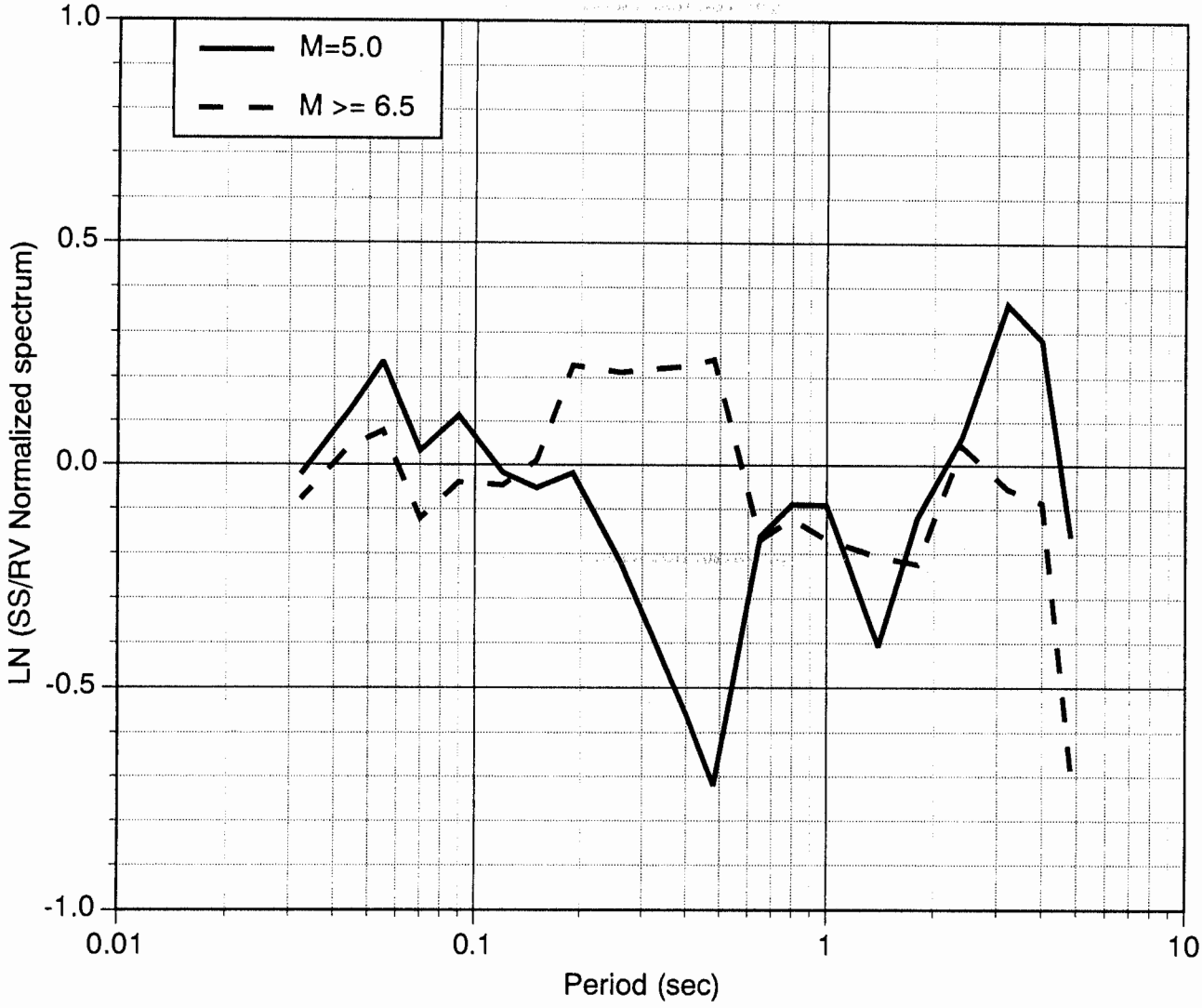

Figure 6. Difference in spectral content between strike-slip and reverse events for all sites characterized by the coefficients a_1 and a_2 derived from normalized spectral shapes. There is not systematic effect that is modeled.

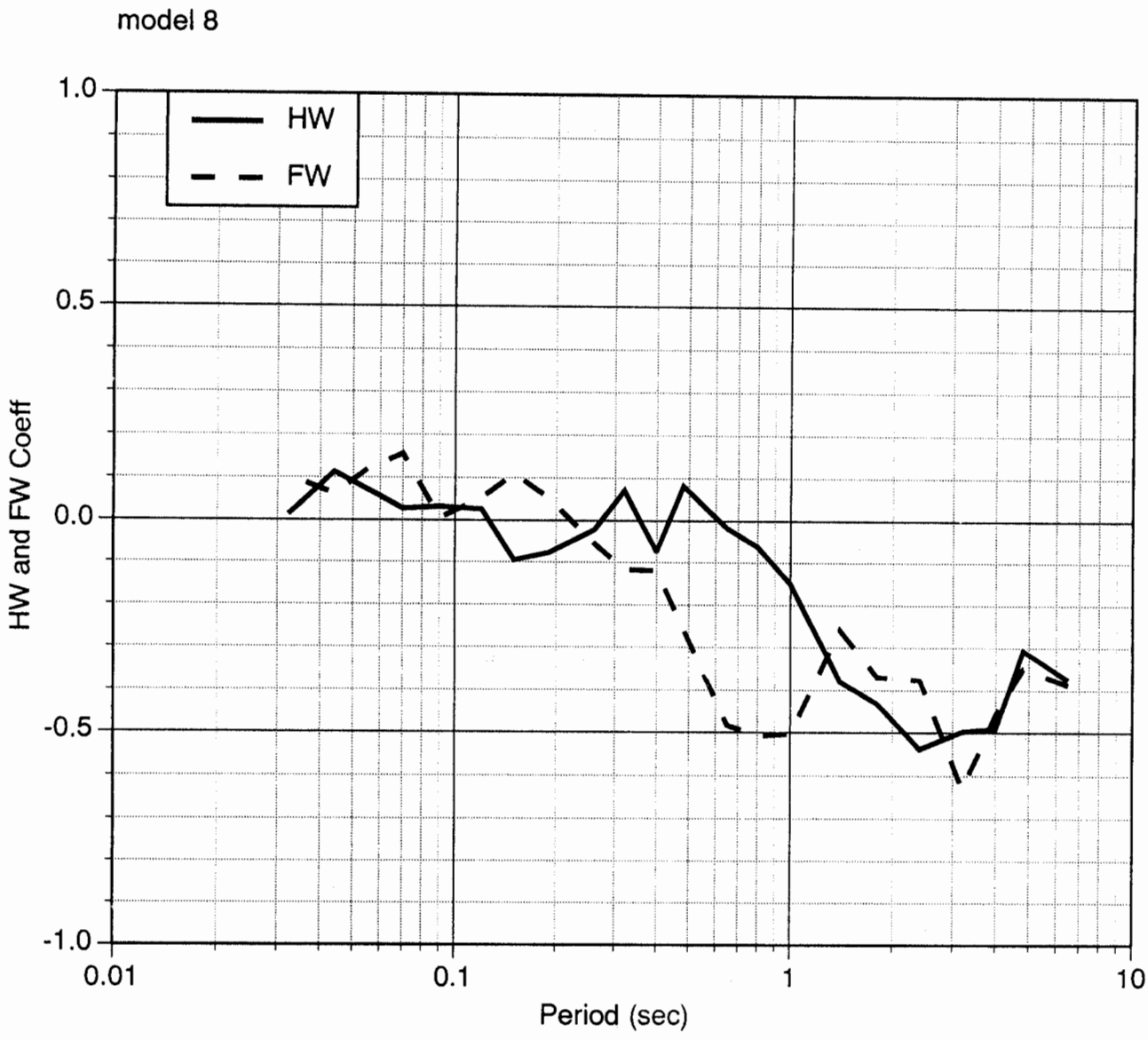

Figure 7. Difference in spectral content between strike-slip and reverse events for sites on the hanging wall and foot wall characterized by the coefficients b_1 and b_2 derived from normalized spectral shapes. This shows a systematic trend of decreasing b_1 and b_2 (HW and FW respectively) at long periods.

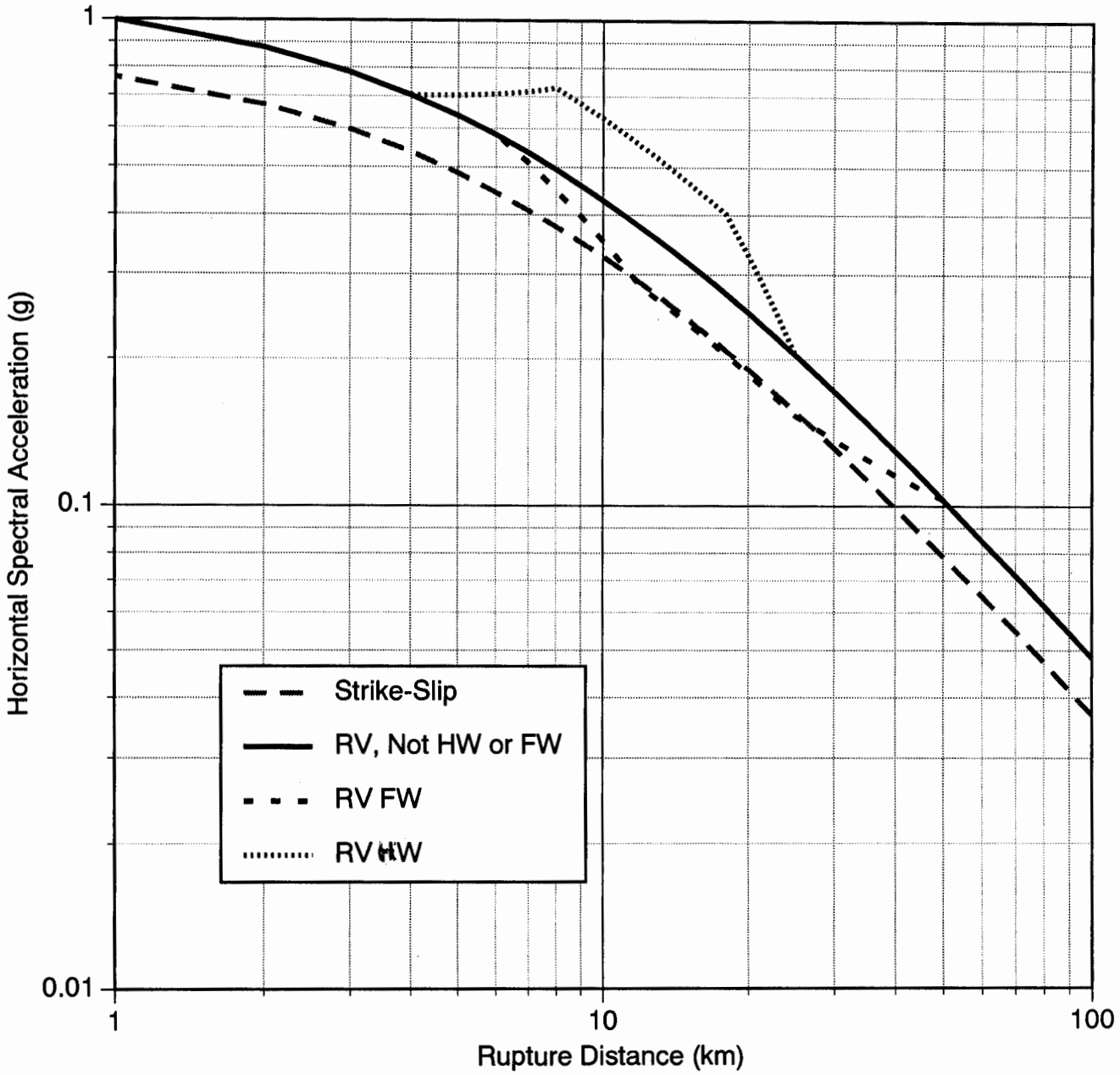

Figure 8A. Median attenuation for peak acceleration for M=7 events.

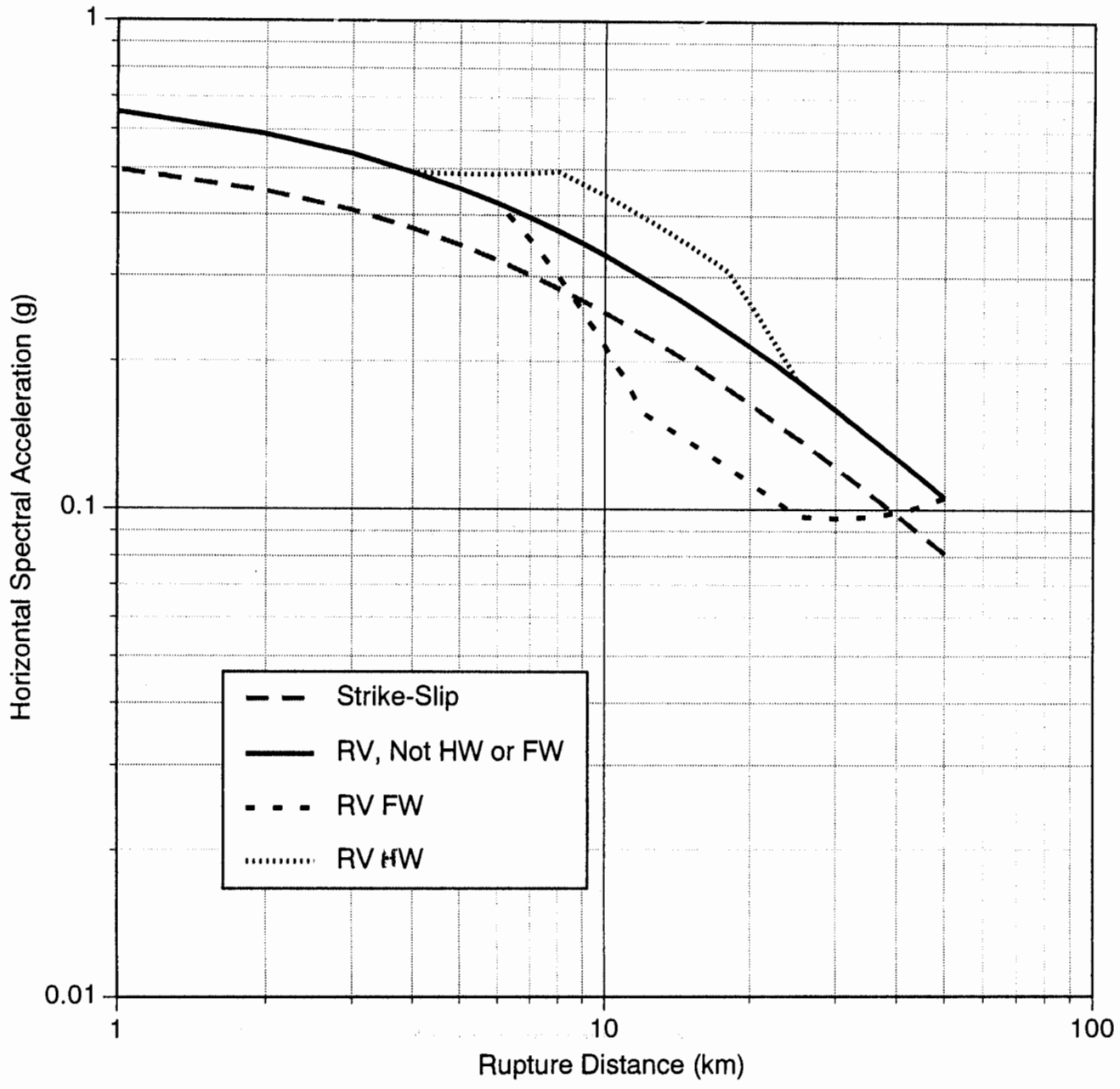

Figure 8. (B) Resulting attenuation relation for 1 Hz spectral acceleration.